Am J Physiol Lung Cell Mol Physiol 309: L821–L833, 2015.
First published August 21, 2015; doi:10.1152/ajplung.00002.2015.

CALL FOR PAPERS | *Nanoparticles and the Lung: Friend or Foe?*

Identification of TGF-β receptor-1 as a key regulator of carbon nanotube-induced fibrogenesis

Anurag Mishra,[1,2] Todd A. Stueckle,[1,2] Robert R. Mercer,[1] Raymond Derk,[1] Yon Rojanasakul,[2] Vincent Castranova,[2] and Liying Wang[1,2]

[1]*Health Effects Laboratory Division (HELD), National Institute for Occupational Safety and Health, Morgantown, West Virginia; and* [2]*Department of Pharmaceutical Sciences, West Virginia University, Morgantown, West Virginia*

Submitted 5 January 2015; accepted in final form 18 August 2015

Mishra A, Stueckle TA, Mercer RR, Derk R, Rojanasakul Y, Castranova V, Wang L. Identification of TGF-β receptor-1 as a key regulator of carbon nanotube-induced fibrogenesis. *Am J Physiol Lung Cell Mol Physiol* 309: L821–L833, 2015. First published August 21, 2015; doi:10.1152/ajplung.00002.2015.—Carbon nanotubes (CNTs) induce rapid interstitial lung fibrosis, but the underlying mechanisms are unclear. Previous studies indicated that the ability of CNTs to penetrate lung epithelium, enter interstitial tissue, and stimulate fibroblasts to produce collagen matrix is important to lung fibrosis. In this study, we investigated the activation of transforming growth factor-β receptor-1 [TGF-β R1; i.e., activin receptor-like kinase 5 (ALK5) receptor] and TGF-β/Smad signaling pathway in CNT-induced collagen production in human lung fibroblasts. Human lung fibroblasts and epithelial cells were exposed to low, physiologically relevant concentrations (0.02–0.6 μg/cm^2) of single-walled CNTs (SWCNT) and multiwalled CNTs (MWCNT) in culture and analyzed for collagen, TGF-β1, TGF-β R1, and SMAD proteins by Western blotting and immunofluorescence. Chemical inhibition of ALK5 and short-hairpin (sh) RNA targeting of TGF-β R1 and Smad2 were used to probe the fibrogenic mechanism of CNTs. Both SWCNT and MWCNT induced an overexpression of TGF-β1, TGF-β R1 and Smad2/3 proteins in lung fibroblasts compared with vehicle or ultrafine carbon black-exposed controls. SWCNT- and MWCNT-induced collagen production was blocked by ALK5 inhibitor or shRNA knockdown of TGF-β R1 and Smad2. Our results indicate the critical role of TGF-β R1/Smad2/3 signaling in CNT-induced fibrogenesis by upregulating collagen production in lung fibroblasts. This novel finding may aid in the design of mechanism-based risk assessment and development of rapid screening tests for nanomaterial fibrogenicity.

carbon nanotubes; collagen I; lung; fibrosis; transforming growth factor; receptor

CARBON NANOTUBES (CNTs) are graphene-based engineered nanoparticles (ENPs), which have generated enormous commercial and biomedical interest owing to their unique physicochemical properties (10). However, increasing evidence has indicated the potential health risks associated with CNT pulmonary exposure, such as lung inflammation and unusual rapid and persistent interstitial fibrosis (22, 24, 30, 37). CNTs have the same morphology as several other high aspect ratio particles, such as asbestos fibers, which are known to induce lung fibrosis. In addition, number of walls, agglomeration, length, surface area, and functionalization have been attributed to their unique fibrogenic response (7, 19, 35). To date, the mechanisms underlying this rapid and progressive interstitial lung fibrosis is not well understood. Identifying such mechanisms is crucial to the understanding of disease pathogenesis and the development of risk assessment and intervention strategies.

Development of interstitial lung fibrosis is a complex process involving numerous cytokines and signaling molecules from multiple cell types, which are released in the interstitial space and stimulate fibroblast production of collagen matrix (30, 41). Upon pulmonary CNT deposition, epithelial cells and macrophages are known to release proinflammatory mediators, such as interleukin-1β (IL-1β), tumor necrosis factor-α (TNF-α), matrix metalloproteinase (MMP), monocyte chemoattractant protein-1, fibroblast growth factor, and transforming growth factor-β (TGF-β), culminating in fibroblast collagen deposition (1, 32, 33, 37). TGF-β1 is a pluripotent cytokine, a central modulator of collagen production in cells, and contributes to both normal and pathological functions of the lung (1–3). Pulmonary exposure to single-walled CNTs (SWCNT) and multiwalled CNTs (MWCNT) significantly elevated the TGF-β1 level in bronchoalveolar lavage fluid of CNT-exposed mice. The CNT-induced response peaked at 7 days postexposure and resulted in progressive pulmonary fibrosis that correlated with lung collagen content (37). Similarly, pulmonary exposure to MWCNT resulted in interstitial particle penetration and TGF-β release, followed by fibrosis (27, 32, 33). Literature suggests that well-dispersed SWCNT exposure resulted in the most potent fibrotic response compared with MWCNT and asbestos fibers on a bulk-mass basis (8). In addition, CNT exposure resulted in transient inflammation but with prolonged fibrosis and biopersistence in interstitial space (23, 24, 30, 37). This suggests that a noninflammatory mechanism of CNT-induced lung fibrosis exists, potentially involving TGF-β1 and direct interaction of interstitial CNTs with lung fibroblasts. These observations imply a link between TGF-β1 signaling and CNT-induced lung fibrosis. Our laboratory previously showed that dispersed SWCNT and MWCNT can directly stimulate human lung fibroblasts to induce collagen production and profibrogenic mediators, such as TGF-β1 and MMP-9 (26, 39).

In lung fibroblasts, binding of TGF-β1 to its receptors results in downstream activation and phosphorylation of intracellular SMAD proteins (15). Among these, Smad2, Smad3, and Smad5 proteins are known to act as transcriptional regulators of several extracellular matrix proteins including collagen (3, 11, 13). In addition to TGF-β1 signaling, other pro-

Address for reprint requests and other correspondence: L. Wang, HELD, National Institute for Occupational Safety and Health, Morgantown, WV 26505 (e-mail: lmw6@cdc.gov).

posed mechanisms of CNT-induced fibrosis include inflammation, oxidative stress, production of other fibrogenic mediators, and epithelial mesenchymal transition. At present, it is not known whether the expression changes in TGF-β1 and/or its receptors (TGF-β R1) play a critical role in Smad signaling, leading to collagen production and the development of rapid and progressive fibrosis induced by CNTs.

The main goal of this study was to utilize relevant in vitro models to complement in vivo animal models and investigate the molecular mechanisms of fibrogenesis induced by SWCNT and MWCNT. We hypothesized that SWCNT and MWCNT exposure to lung epithelial and fibroblast cells would enhance the release of TGF-β1 and activate the TGF-β1/Smad pathway in fibroblast cells, culminating in enhanced collagen I production. Furthermore, we hypothesized that blocking the TGF-β R1/Smad pathway would reduce collagen induction by CNTs in fibroblast cells. Elucidating the role of this pathway in CNT-induced fibrogenesis will assist in risk assessment and development of safer nanomaterials. In addition, this study will provide added framework for development of rapid in vitro-based prediction and screening of fibrogenic nanoparticles.

MATERIALS AND METHODS

Reagents. Dulbecco's modified Eagle's medium (DMEM), phosphate-buffered saline (PBS), trypsin, fetal bovine serum (FBS), and penicillin-streptomycin antibiotic solution were purchased from Sigma-Aldrich (St. Louis, MO). Eagle's minimum essential medium (EMEM) was purchased from American Type Culture Collection (ATCC, Manassas, VA). TGF-β R1 [activin receptor-like kinase (ALK)-5 blocker], SB431542, was purchased from Tocris Bioscience (Minneapolis, MN). Smad3 inhibitor (SIS3) and short hairpin (sh)RNA lentiviral particles for TGF-β R1, Smad2, Polybrene, and puromycin hydrochloride were purchased from Santa Cruz Biotechnology (Santa Cruz, CA). Antibodies for pSmad2/3 (sc-11769), TGF-β1 (sc-146), TGF-β R1 (sc-398), and Smad2 (sc-6200) were obtained from Santa Cruz Biotechnology. Collagen I antibody (70R-CR007x) was obtained from Fitzgerald (Concord, MA).

Cell culture and CNT dispersion. Human lung bronchial epithelial BEAS-2B cells and lung fibroblast CRL-1490 cells (ATCC) were grown in DMEM and EMEM, respectively. Each cell type's medium contained 5% FBS, 100 U/ml penicillin-streptomycin, and 1% wt/vol L-glutamine. Cells were cultured and kept at subconfluent densities in a humidified incubator at 37°C with 5% CO_2. Prior to characterization and exposure studies, dry CNTs were suspended in PBS containing 150 μg/ml of Survanta to obtain 0.1 mg/ml stock solutions. Survanta, a commercially available lung surfactant, was previously validated to disperse CNTs for in vitro toxicity testing, which mimics aerosolized and inhaled dispersed CNTs found in vivo and shows no stimulatory or cytotoxic effects (26, 39). Particle stock solutions were briefly sonicated to disperse each particle and then diluted with culture medium to achieve physiologically relevant concentrations (0.02, 0.06, 0.2, 0.6 μg/cm^2) as described previously (39).

Nanoparticle source and characterization. SWCNT (CNI, Houston, TX) were produced by high pressure carbon monoxide (CO) disproportionation (HiPco) technique, employing CO in a continuous-flow gas phase as the carbon feedstock and $Fe(CO)_5$ as the iron-containing catalyst precursor. These SWCNT were purified by acid treatment to remove metal contaminates; we fully characterized these SWCNT for physicochemical properties in a previous study (34). Elemental analysis of the supplied SWCNT by nitric acid dissolution and inductively coupled plasma-atomic emission spectrometry (ICP-AES, NMAM no. 7300) showed that the SWCNT were 99% elemental carbon and 0.23% iron. The specific surface area was measured at −196°C by the nitrogen absorption-desorption technique (Brunauer Emmet Teller method, BET), using a SA3100 Surface Area and Pore Size Analyzer (Beckman Coulter, Fullerton, CA). The surface area of dry SWCNT was 1,040 m^2/g, and the length and width of individual (dry) SWCNT were 0.1–1 μm and 0.8–1.2 nm, respectively. MWCNT used in this study were obtained from Mitsui (XNRI MWNT-7, lot no. 05072001K28) and were fully characterized in a previous report (30). Briefly, MWCNT trace metal contamination was 0.78%, with sodium (0.41%) and iron (0.32%) being the major metal contaminants. Average MWCNT surface area measured by BET was 26 m^2/g (30). Elftex 12 ultrafine carbon black (UFCB) was acquired from Cabot (Edison, NJ) and was previously characterized by our laboratory (38). Briefly, it possesses >99% carbon and 0.0011% iron, 37 nm dry mean width, and 43 m^2/g surface area.

The diameter and length distribution of poorly and well-dispersed preparations of UFCB, SWCNT, and MWCNT (without or with Survanta dispersal agent) in culture medium were measured by field emission scanning electron microscopy (FESEM) (26, 38). Briefly, dispersed particles were suspended in culture medium (0.2 μg/cm^2) and filtered through polycarbonate filter to collect dispersed particles. Dried samples were mounted, gold/palladium sputter coated, and imaged at ×400 and ×30,000 magnification. Length and width measurements of >300 particles from three independent replicates were performed. Survanta-dispersed SWCNT structure exhibited mean count dimensions (length and width) of 1.08 μm × 0.27 μm (39), while MWCNT structure exhibited 5.1 μm × 0.078 μm mean dimensions (26). The UFCB dispersed in Survanta had mean length 930 nm and width 700 nm (38). The same concentration of Survanta alone (150 μg/ml) and PBS alone were used as dispersant controls.

Cytoviva hyperspectral imaging. To assist in visualization of uptake and fate of CNTs, CRL-1490 cells were plated at a density of 30,000 cells/ml on glass coverslips and exposed to 0.1 μg/cm^2 of SWCNT and MWCNT. After 24 h of exposure, cells were washed with PBS, fixed with 4% formaldehyde, and stained with 1% toluidine blue dye. Representative micrographs of SWCNT- and MWCNT-exposed cells were taken using dark-field-enhanced and hyperspectral microscopy (Cytoviva, Auburn, AL). Cytoviva technology was specifically designed for optical observation and spectral confirmation of NPs as they interact with cells and tissues. Scattered light form nanoparticles is detectable with dark-field-enhanced imaging and can be discerned from low scattered light from cells and tissues. The system is capable of identifying specific material at sub 100-nanometer resolution based on the material's unique spectral signature. Scattered light and hyperspectral images of CNT-treated cells were captured with an integrated CCD camera and the Cytoviva spectrophotometer mounted on an Olympus BX-51 microscope, and spectra from specific materials were acquired and analyzed. Briefly, spectral libraries for UFCB, SWCNT, and MWCNT were generated using enhanced-dark-field imaging. Next, cells with CNT and UFCB were scanned and each pixel of a scanned image was compared with the spectral library of nanoparticles and color-coded for pixel location. Finally, images were compared with dual-mode fluorescence images stained for F-actin (phalloidin) and nucleus (DAPI). The images were compared to determine the location of intracellular nanoparticles.

Animal exposure. Pathogen-free C57BL/6 mice (Jackson, Bar Harbor, ME) were used for animal studies. Mice were housed in an AAALAC-accredited, specific-pathogen-free, environmentally controlled facility and allowed to acclimate at least 1 wk prior to use. All experimental procedures were conducted in accordance with a protocol (no. 11-LR-M-018) approved by the Institutional Animal Care and Use Committee of West Virginia University and met current National Institutes of Health guidelines for animal care and handling. Mice were kept in laminar-flow cages, which were provided HEPA-filtered air with Teklad 7913 hardwood Beta-Chips for bedding. Food and tap water were given ad libitum. The animals were exposed by pharyngeal aspiration. They were anesthetized by an intraperitoneal injection of ketamine and xylazine (45 and 8 mg/kg ip) and placed on a board in the supine position. The animal's tongue was extended with padded

forceps. A suspension of dispersed UFCB, SWCNT, MWCNT (at 40 μg/100 μl per mouse), or saline was placed on the back of the tongue. The tongue was restrained until at least two deep breaths were completed. Mice were euthanized at 4 wk after the treatment via intraperitoneal injection of pentobarbital sodium (>100 mg/kg body wt ip) followed by exsanguination. The lungs were immediately collected, homogenized, and lysed on ice with RIPA buffer, centrifuged at 13,500 rpm for 30 min to obtain supernatants, and stored at −70°C. Whole lung supernatants were assayed for collagen I expression by Western blotting as described below.

Lung fixation and section preparation. At 28 days after pharyngeal aspiration of the particles, mice were euthanized by an overdose of pentobarbital sodium (>100 mg/kg body wt ip) followed by transection of the abdominal aorta to provide exsanguination. The right lungs were removed from the chest cavity, placed in tubes, and frozen at −80°C for protein expression analysis. The remaining trachea were cannulated and the left lungs were inflated and fixed by intratracheal perfusion with 1 ml of 10% neutral buffered formalin and embedded in paraffin. For histology, paraffin sections of the left lung (5 μm thick) were cut. The sections were then deparaffinized and rehydrated with xylene-alcohol series to distilled water. To enhance the contrast between tissue and CNTs, lung sections were stained with Sirius Red. Sirius Red staining consisted of immersion of the slides in 0.1% Picrosirius solution (100 mg of Sirius Red F3BA in 100 ml of saturated aqueous picric acid, pH 2) for 1–2 h followed by washing for 1 min in 0.01 N HCl. Sections were then briefly counterstained in freshly filtered Mayer's hematoxylin for 2 min, dehydrated, and mounted on a slide with a coverslip.

Western blotting. Cells were washed two times with ice-cold PBS, lysed with cell lysis buffer (Invitrogen, Carlsbad, CA) in the presence of protease inhibitor mixture (Roche Diagnostics, Indianapolis, IN), and incubated for 30 min on ice. Cell lysates were scraped off the plates, collected into tubes, and centrifuged for 10 min at 13, 200 *g* at 4°C. Supernatants were collected and stored at −70°C until further use. Total protein concentration of the supernatant was determined using the bicinchoninic acid protein assay kit (Pierce, Rockford, IL), using bovine serum albumin standard following the manufacturer's instructions. Next, 20 μg of proteins were resolved on 10% bis-Tris gels using a Bio-Rad system. Protein was transferred to nitrocellulose membrane using semi-dry transfer system (ThermoFisher Scientific, Lafayette, CO). The membrane was blocked for 1 h at room temperature in 5% non-fat dry milk in Tris buffer with 0.1% Tween 20 (TBST) and incubated with primary antibody at 4°C overnight. Chemiluminescence detection was performed using horseradish peroxidase-tagged secondary anti-rabbit (sc-2004) or anti-mouse antibody (sc-2005; Santa Cruz Biotechnology) followed by 5 min of incubation in SuperSignal West Pico or Femto Chemiluminescent Substrate (ThermoFisher Scientific) and exposure to film. The membrane was washed 3 times for 10 min in TBST following both primary and secondary antibody incubations.

Chemical inhibition and shRNA lentiviral transfection. Cells were preincubated with 5 μM SB431542 for 3 h to block the ALK5 receptor, then exposed to SWCNT or MWCNT (0.02, 0.06, 0.2 μg/cm^2) for 48 h. SB431542 is a well-characterized, specific, and potent ALK5 blocker that prevents binding of activated TGF-β to the receptor, thus preventing signaling cascade activation (16). No SB431542-pretreated cells with the same CNT treatments served as controls. In addition, CRL-1490 cells were transfected with 10–20 μl of lentiviral particles (1.0×10^6 infection units/ml), according to the manufacturer's recommendations. Briefly, the cells were seeded in 12-well plates in EMEM media containing 10% FBS. After 24 h, complete medium with Polybrene (5 μg/ml) was added, and cells were infected with shRNA lentiviral particles. Stable colonies were selected and expanded using puromycin (Santa Cruz, CA). To confirm

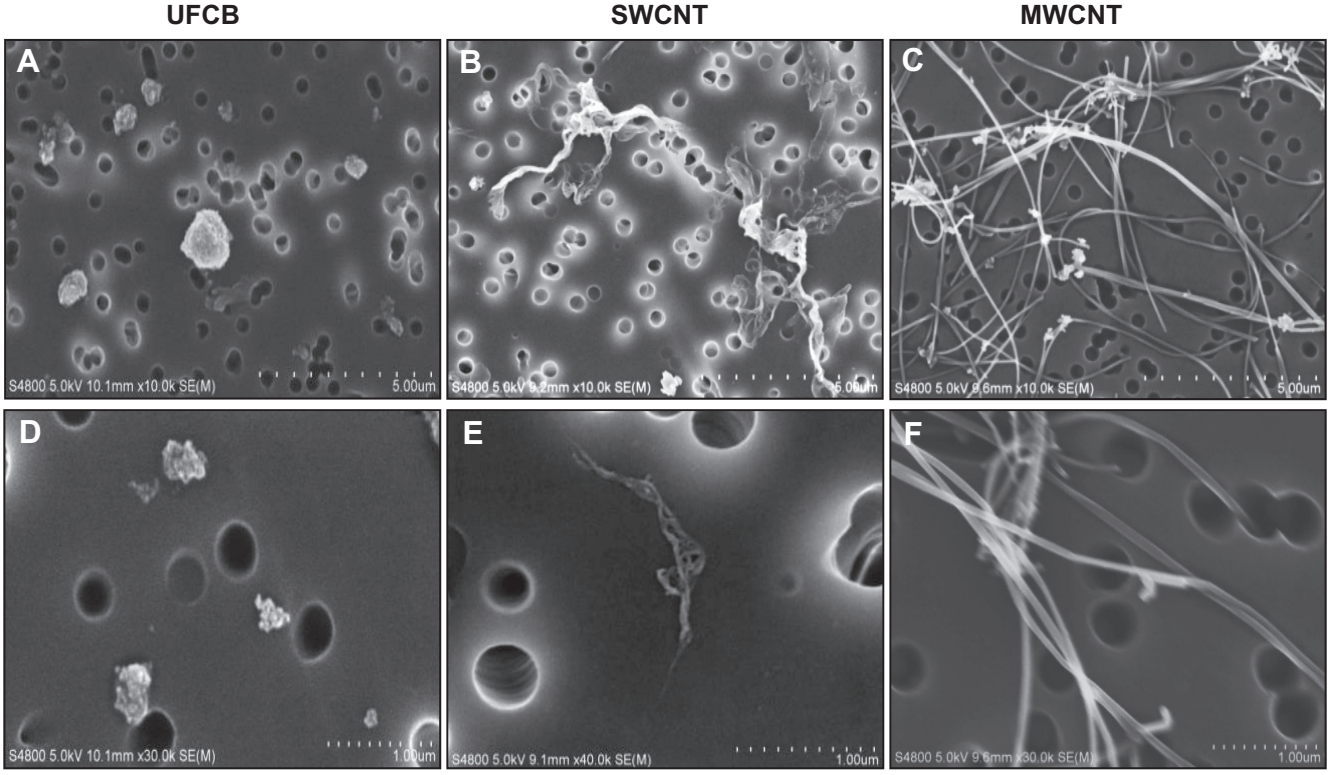

Fig. 1. Particle characterization of dispersed ultrafine carbon black (UFCB), single-walled carbon nanotubes (SWCNT), and multiwalled CNT (MWCNT). Field emission scanning electron micrographs of Survanta-dispersed UFCB (*A* and *D*), Survanta-dispersed SWCNT (*B* and *E*), and Survanta-dispersed MWCNT (*C* and *F*) at low (*top*, 5 μm) and high (*bottom*, 1 μm) magnification. Micrographs of SWCNT and MWCNT show distinct fiber-shaped morphology compared with spherical shape UFCB particles.

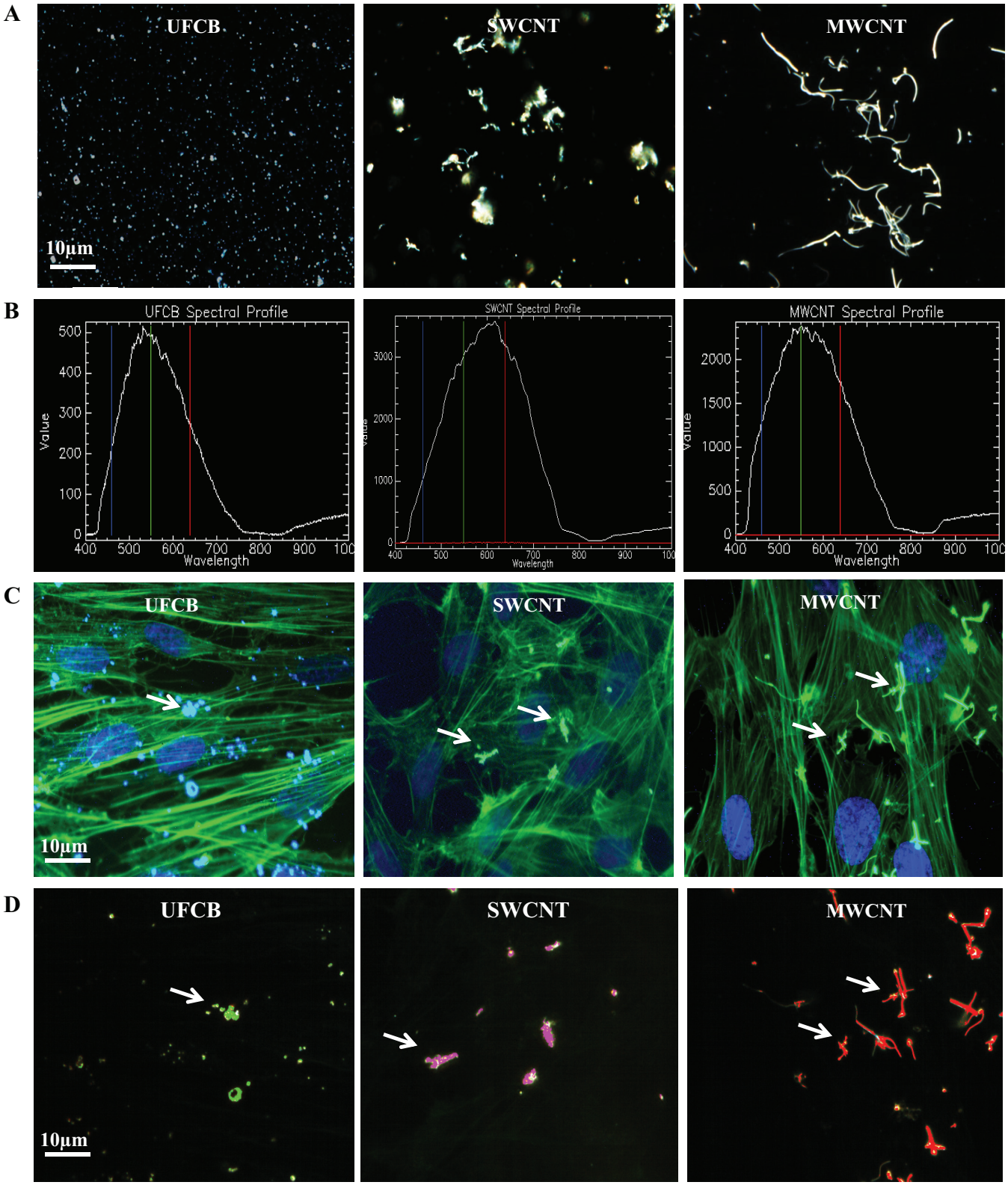

Fig. 2. Hyperspectral imaging of CNT-exposed human lung fibroblast cells. *A* and *B*: enhanced dark-field images (*A*) and hyperspectral signatures (*B*) of UFCB, SWCNT, and MWCNT. *C*: human lung fibroblast cells were exposed to UFCB, SWCNT, and MWCNT and stained with phalloidin dye for F-actin (green) and DAPI for nucleus (blue). *D*: Cytoviva hyperspectral imaging confirming the presence of UFCB (green), SWCNT (pink), and MWCNT (red) in the cells. White arrows indicate carbon nanomaterial associated with lung fibroblasts. Representative images are from $n = 5$ independent experiments with at least 100 cells per condition in each experiment.

shRNA gene knockdown, protein expression was analyzed by Western blotting as described above.

ELISA. For analysis of secreted TGF-β1, lung fibroblast (CRL-1460) cells were plated (1×10^5) and were exposed to CNTs (0.02–0.2 μg/cm^2) in DMEM medium with 2% FBS for 48 h. Postexposure cell supernatants were collected and analyzed using an ELISA kit (R&D, Minneapolis, MN). Briefly, 100 μl of cell culture supernatant was mixed with 1 N HCL and 1.2 N NaOH/0.5 M HEPES to activate latent TGF-β1 and added to pre-antibody-coated 96-well plates for 2 h, after which biotinylated peroxidase-conjugated secondary antibody was added (2 h) and the reaction was stopped by addition of an acid solution. The plate was then read for absorbance at 450 nm (Molecular Device Spectra max 250, Sunnyvale, CA).

Immunofluorescence. To determine TGF-β R1 and Smad2 localization in cells following CNT exposure, fibroblast cells were plated onto glass coverslips at a density of 30,000 cells/ml with 1 ml of cell suspension being added to each well. The next day, cells were supplied with appropriate fresh medium and exposed to 0.2 μg/cm^2 of SWCNT and MWCNT for 48 h. After exposure, the cells were washed 3 times for 5 min each at room temperature with PBS, followed by fixation for 15 min in 1 ml of 4% paraformaldehyde. Cells were then washed 3 times for 5 min each in PBS, followed by permeabilization with 0.5 ml of 0.1% Triton X-100 for 5 min. After permeabilization, the cells were washed 3 times for 5 min each with PBS, followed by blocking with 5% goat serum for 30 min. The serum was then removed, and 450 ml of a 2% goat serum-PBS solution containing a 1:200 dilution of primary antibody were added and incubated at 4°C overnight. The primary antibodies used were Smad2 (sc-8332; Santa Cruz Biotechnology) and TGF-β R1 (Cell Signaling, Danvers, MA). Cells were then washed 3 times for 5 min in PBS and further incubated with 300 μl of a 2% goat serum-PBS solution containing a 1:400 dilution of a species-specific Alexa-488 labeled secondary antibody (Cell Signaling). After incubation for 2 h, the cells were washed 3 times for 5 min at room temperature with PBS and slides were mounted with Prolong gold antifade reagent (Life Technologies, Grand Island, NY). Images were captured, using an E800 Nikon microscope configured with DAPI and FITC fluorescence excitation filters and equipped with Spot RTs digital camera and Meta Morphs 4.5 software image analysis package (Universal Imaging, West Chester, PA).

Statistical analysis. One- and two-way ANOVA followed by post hoc tests were performed to determine statistical significance between treatments using GraphPad Prism software (version 5.1; GraphPad Software, La Jolla, CA) at a confidence level of $P < 0.05$. Either a Dunnett's or Tukey-Kramer honestly significant difference (HSD) post hoc test was conducted when the ANOVA result indicated a significant difference among means.

RESULTS

Carbon nanotube characterization and interaction with human lung epithelial cells. To assess the morphology and aggregation state of dispersed ultrafine carbon black (UFCB), single-walled carbon nanotubes (SWCNT), and multiwalled carbon nanotubes (MWCNT) in culture medium, field emission scanning electron microscopy (FESEM) was employed. As shown in Fig. 1, compared with UFCB (*A* and *D*), SWCNT (*B* and *E*) and MWCNT (*C* and *F*) showed distinct fiber shape morphology. Comparison of FESEM images reveals that MWCNT fibers had straight needle-shaped morphology, whereas SWCNT bundles were more flexible. Dispersed particle characteristics matched our previously reported size distribution analysis using FESEM (22, 26, 39). The UFCB dispersed in Survanta had a mean length of 930 nm and width of 700 nm. The count median width (CMW) of dispersed SWCNT and MWCNT agglomerates was 0.27 and 0.078 μm, whereas count median length (CML) was 1 μm and 5.1 μm, respectively.

Cellular internalization of UFCB, SWCNT, and MWCNT by hyperspectral imaging. Next, association of each particle was evaluated in human lung fibroblast CRL-1460 cells after 24 h of exposure. A dark-field image of UFCB, SWCNT, and MWCNT confirms fibrous morphology of SWCNT and MWCNT, which was distinct from the spherical UFCB particles (Fig. 2*A*). Spectral libraries were created for UFCB, SWCNT, and MWCNT, where each spectrum in the library represents a single pixel and is a characteristic signature of the particular nanoparticles (Fig. 2*B*). Human fibroblast cells exposed to UFCB, SWCNT, and MWCNT (0.02 μg/cm^2) were stained for F-actin, and the DNA exhibited healthy morphology and adherence. The same fields of view were imaged in enhanced-dark-field mode (Fig. 2*D*) to confirm the internalization of nanomaterials within the cytoplasm. As shown in Fig. 2*D*, spectral matching was confirmed in human fibroblast cells for UFCB (green), SWCNT (pink), and MWCNT (red). Moreover, SWCNT and MWCNT exist as fibrous particles colocalized with human fibroblast cells compared with UFCB. Cellular uptake data confirmed direct cell-nanoparticle interaction and internalization. This result suggests that CNTs are internalized into human lung fibroblasts and epithelial cells at 24 h postexposure.

SWCNT and MWCNT induce collagen I and TGF-β1 in mouse lungs and cultured cells. To verify the in vivo fibrogenic effect of SWCNT and MWCNT, mice were exposed by pharyngeal aspiration to UFCB, SWCNT, and MWCNT (40 μg/mouse) compared with dispersant-only as a vehicle control. At 4 wk posttreatment, mice were euthanized and the lungs were lysed or fixed and analyzed for collagen content, a hallmark of lung fibrosis. Figure 3*A* shows that SWCNT and MWCNT significantly induced a 3.5- to 4-fold increase in lung collagen content compared with UFCB and dispersant-only controls ($P < 0.05$) while representative lung tissue images showed correlated thickening of the alveolar wall and increased collagen (stain by Sirius Red) in SWCNT- and MWCNT-exposed lung tissue (Fig. 3*B*). Such data are consistent with previous

Fig. 3. Dispersed SWCNT and MWCNT induce in vivo and in vitro collagen I and in vitro transforming growth factor-β1 (TGF-β1) production. *A*: SWCNT and MWCNT induced a significant increase in collagen I production in animal lungs compared with UFCB or dispersant-only treated control (CL) animals at 4 wk posttreatment. Representative blots are from $n = 3$ independent experiments. *B*: light micrographs of lung sections showing SWCNT- and MWCNT-induced alveolar thickness and collage I deposition compared with control lung. Black arrows indicate CNT deposition in lung interstitium. Collagen fibers are red in the section due to staining with Sirius Red. *C* and *D*: human lung fibroblast CRL-1490 cells were exposed to UFCB, SWCNT, and MWCNT (0.2 μg/cm^2) for 48 h. Endogenous collagen I (130 kDa), endogenous TGF-β1 (25 kDa), and loading control β-actin levels were measured by Western blot. Representative blots are from $n = 4$ independent experiments. *E*: secreted TGF-β1 levels in the culture medium were measured by ELISA following a 48-h exposure of CRL-1490 cells to dispersant-only control (CL), 0.2 μg/cm^2 UFCB, or the indicated doses of SWCNT and MWCNT. Each bar represents the mean ± SD (6 mice/group) or $n = 4$ independent in vitro experiment. *$P < 0.05$ vs. dispersant-only control, #$P < 0.05$ vs. SWCNT.

observations (21, 23, 37). To determine a similar in vitro fibrogenic effect of CNTs, cultured human lung fibroblast CRL-1490 cells were treated with 0.2 μg/cm^2 of the same material (SWCNT, MWCNT, and UFCB) for 48 h. Endogenous levels of collagen I, TGF-β1, and β-actin were measured by Western blotting. Collagen I (Fig. 3*C*) expression was significantly increased 3.5- and 2-fold in SWCNT- and MWCNT-exposed cells, respectively ($P < 0.05$) compared with

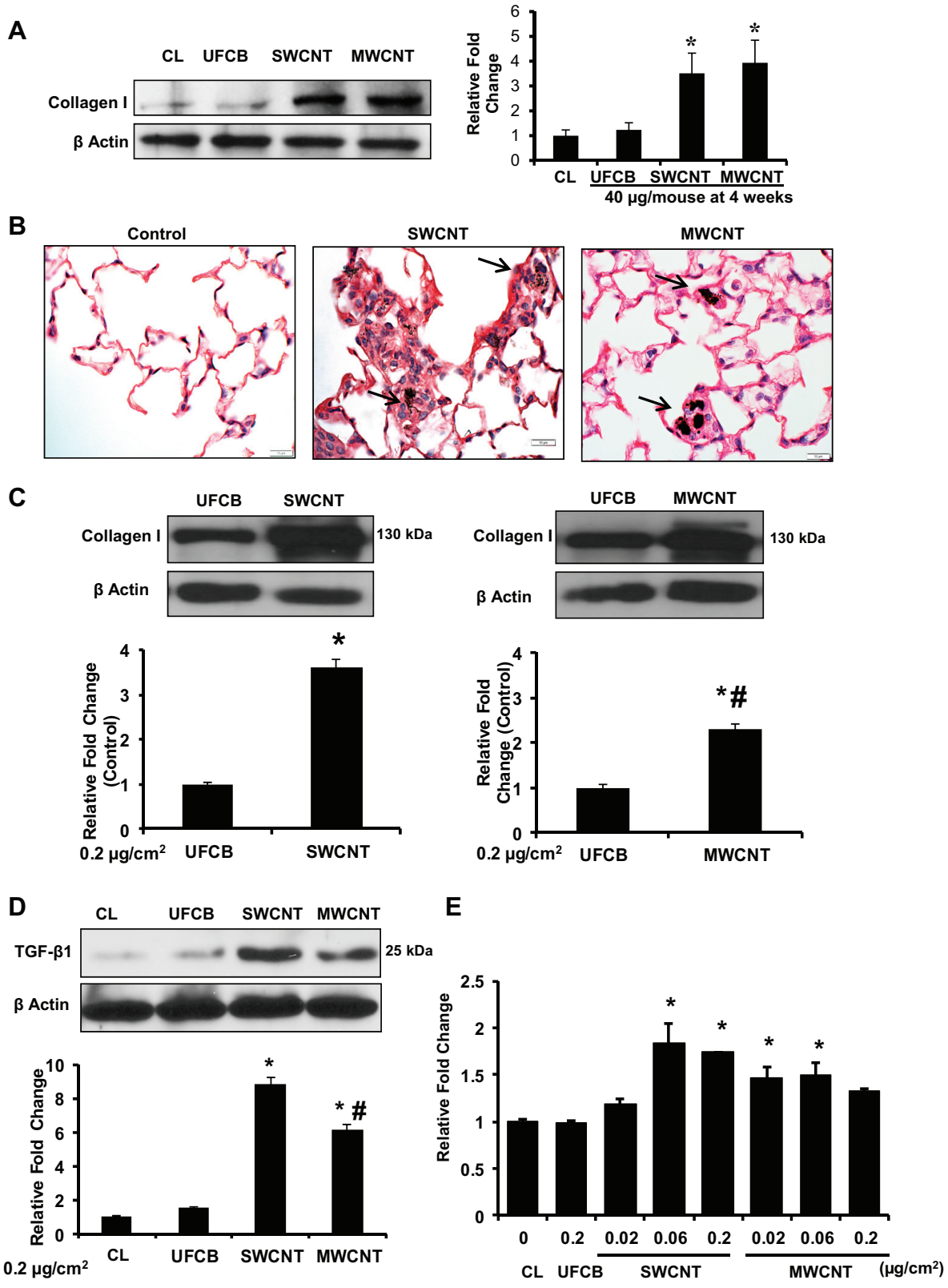

UFCB-exposed cells. Similarly, TGF-β1 total protein levels exhibited 8- and 6-fold upregulation in SWCNT- and MWCNT-exposed fibroblasts (CRL-1490), respectively (Fig. 3*D*). In addition, significantly higher levels of TGF-β1 were secreted by SWCNT- or MWCNT-exposed fibroblast cells compared with dispersant-only and UFCB-treated cells (Fig. 3*E*). Of note, SWCNT-exposed fibroblast cells exhibited a trend for greater TGF-β1 and collagen I expression than MWCNT-exposed cells.

Previously, we reported that MWCNT exposure to epithelial BEAS-2B cells resulted in a dose-dependent increase in secreted TGF-β1 (26). Similarly, BEAS-2B cells were treated with 0.02–0.2 μg/cm^2 of SWCNT and 0.2 μg/cm^2 of UFCB as a control for 48 h and evaluated for secreted TGF-β1 in cell supernatants. A significant increase in secreted TGF-β1 was observed in SWCNT-exposed cells compared with no treatment and UFCB controls (data not shown). These results are consistent with the in vivo induction of TGF-β1 in CNT-

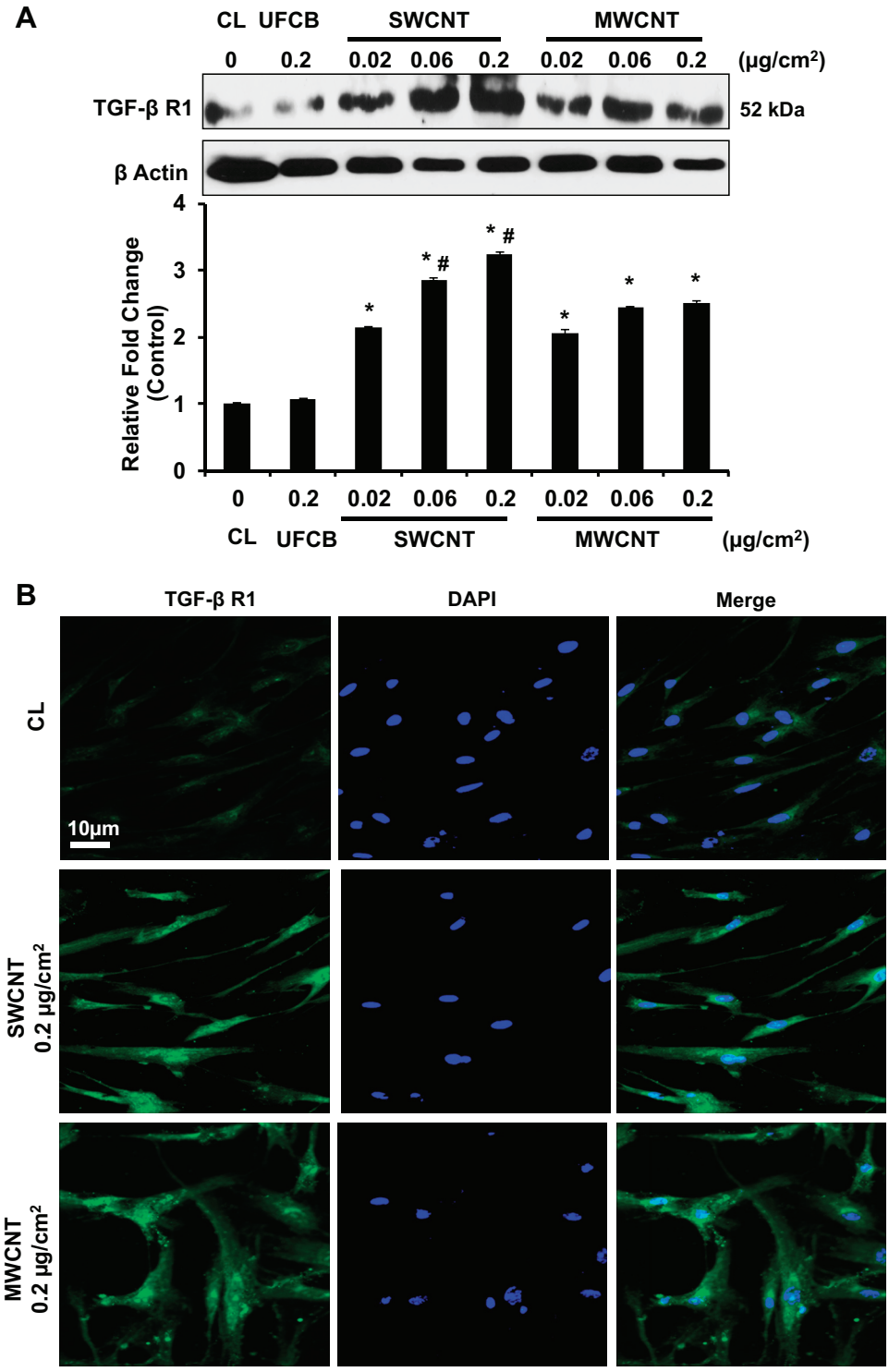

Fig. 4. Effect of SWCNT and MWCNT treatment on human lung fibroblast TGF-β receptor-1 (TGF-β R1) expression. *A*: lung fibroblast CRL-1490 cells were treated with 0.02–0.2 μg/cm^2 of SWCNT and MWCNT, respectively, for 48 h, and endogenous TGF-β R1 levels (56 kDa) in the cell lysates were measured by Western blotting and compared with dispersant-only control (CL) and UFCB (0.2 μg/cm^2)-treated cells. Representative blots are from $n = 3$ independent experiments. *B*: CRL-1490 were exposed to 0.2 μg/cm^2 of SWCNT (*middle*) or MWCNT (*bottom*) for 48 h and stained with TGF-β R1 antibody followed by FITC-tagged secondary antibody. Immunofluorescence imaging of the treated cells and dispersant-only treated control is shown. DAPI was used to stain cell nucleus. Representative images are from $n = 3$ independent experiments with at least 100 cells per condition in each experiment. Each bar represents the mean ± SD for $n = 3$ independent experiments. *$P < 0.05$ vs. dispersant-only control (CL), #$P < 0.05$ vs. SWCNT or MWCNT-treated cells. Scale bar, 10 μm.

exposed mouse lung lavage fluids (37) and support the predictive value of the in vitro data.

Carbon nanotubes induce TGF-β receptor-1 in human lung fibroblasts. The same CNT-treated and control fibroblast cells described in Fig. 3 were also investigated for TGF-β R1 expression by Western blotting. Densitometry analysis indicated that cells exposed to SWCNT and MWCNT induced significant dose-dependent increases (≥2-fold) in TGF-β R1 expression compared with those exposed to UFCB or dispersant-only controls (Fig. 4*A*). In addition, SWCNT exposure resulted in a significantly higher ($P < 0.05$) TGF-β R1 level than MWCNT at the doses of 0.06 and 0.2 μg/cm^2. Immunofluorescence imaging showed TGF-β R1 overexpression at the cellular periphery of SWCNT- and MWCNT-exposed cells compared with dispersant-only controls, which showed either basal cytoplasmic or concentrated TGF-β R1 in the nuclei (Fig. 4*B*). The upregulation of TGF-β R1 is consistent with CNT-induced TGF-β1 in both lung epithelial and fibroblast cells and suggests the involvement of a TGF-β signaling pathway in CNT-induced lung pathogenesis.

Chemical inhibition and knockdown of TGF-β receptor-1 reduces CNT-induced collagen I expression in lung fibroblasts. TGF-β1 binds to TGF-β1 receptor (ALK5) and activates the downstream signaling pathway involving Smad proteins, lead-

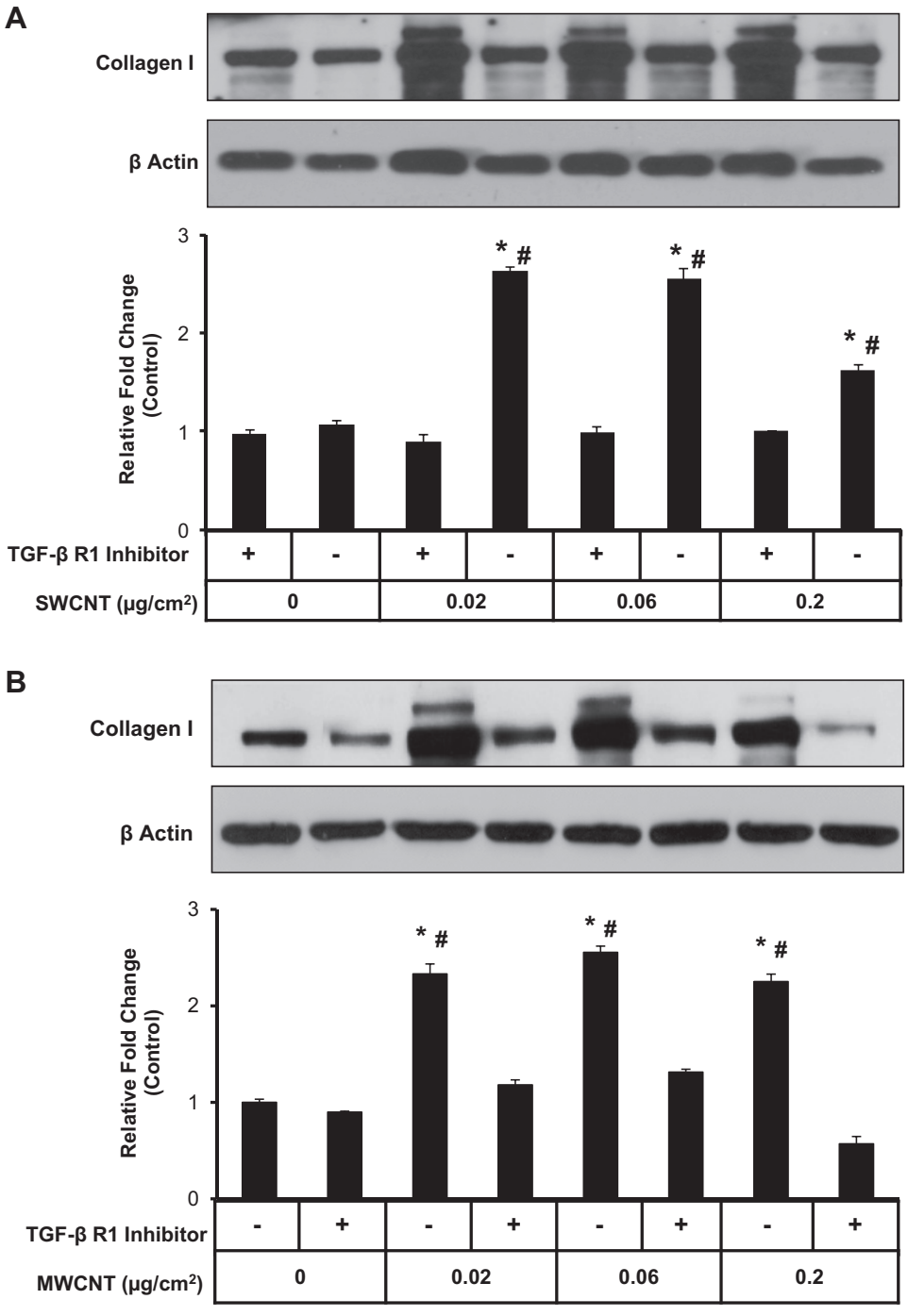

Fig. 5. Effect of TGF-β R1 [activin receptor-like kinase (ALK)-5] chemical inhibitor on CNT-induced collagen production. Human lung fibroblast CRL-1490 cells were exposed to 5 μM TGF-β R1 (ALK5) inhibtor (SB431542) for 3 h, then treated with SWCNT (*A*) or MWCNT (*B*) at concentrations of 0.02 to 0.2 μg/cm^2. At 48 h post-CNT exposure, collagen I production was measured by Western blotting and compared with dispersant-only or inhibitor-only treated control cells. Representative blots are from $n = 3$ independent experiments. Each bar represents the mean ± SD for $n = 3$ independent experiments. *$P < 0.05$ vs. control, #$P < 0.05$ vs. pretreated TGF-β R1 inhibitor-only cells.

ing to collagen synthesis. To ascertain the role of TGF-β R1 in CNT-induced fibroblast collagen production, TGF-β R1 was inhibited using a known chemical inhibitor of the receptor, SB431542. Treatment of lung fibroblasts with the inhibitor strongly decreased SWCNT- and MWCNT-induced collagen production (>2-fold; $P < 0.05$; Fig. 5, *A* and *B*). This finding suggests a critical role of TGF-β R1 in the fibrogenic effect of SWCNT and MWCNT in exposed lung fibroblasts.

shRNA are small interfering RNA, which can knock down specific gene expression by interfering with its mRNA. To confirm the effect of chemical inhibition of TGF-β R1 on CNT-induced collagen production in lung fibroblasts (Fig. 5), TGF-β receptors were knocked down in fibroblasts using lentiviral particles carrying shRNA against TGF-β R1 (sh-TGF-β R1). Lentiviral particles carrying empty vector shRNA were used as a control (sh-Control). Figure 6*A* shows successful knockdown of TGF-β R1 protein in sh-TGF-β R1-treated cells compared with sh-Control cells. Next, sh-TGF-β R1 and sh-Control cells were exposed to SWCNT and MWCNT (0.2 μg/cm^2) for 48 h and analyzed for collagen I expression by Western blotting. Figure 6, *B* and *C*, shows that collagen I expression was substantially (4- to 5-fold) lower in sh-TGF-β R1 cells compared with sh-Control cells ($P < 0.05$), supporting the role of TGF-β R1 in CNT-induced fibroblast production of collagen.

Activation of Smad2 by carbon nanotubes. Smad proteins are intracellular proteins that transduce extracellular signals from TGF-β ligands to nucleus where they activate downstream TGF-β gene transcription. Receptor-regulated Smad2 is activated by phosphorylation. As shown in Fig. 7*A*, SWCNT and MWCNT (0.02–0.2 μg/cm^2) dose dependently induced Smad2 phosphorylation (p-Smad2) in lung fibroblasts compared with UFCB and no treatment controls. To determine the intracellular localization of p-Smad2 in CNT-exposed cells, immunofluorescence staining of p-Smad2 protein was performed. Figure 7*B* shows nuclear localization (red arrow) of p-Smad2 protein in SWCNT- and MWCNT-exposed cells compared with control cells. These results suggest the involvement of Smad2 activation in human lung fibroblasts following CNT exposure.

Knockdown of Smad reduces CNT-induced collagen expression in lung fibroblasts. To further determine the role of Smad2 in CNT-induced collagen production in lung fibroblasts, Smad2 knockdown cells were generated using lentiviral particles carrying Smad2 shRNA (sh-Smad2). A 2-fold reduction of Smad2 protein was evident in the sh-Smad2-treated cells (Fig. 8*A*) compared with shRNA control (sh-Control) cells. Stable sh-Smad2 and sh-Control cells were exposed to SWCNT or MWCNT (0.2 μg/cm^2) for 48 h and analyzed for collagen I expression by Western blotting. Figure 8*B* shows a significant 2-fold reduction of collagen I expression in sh-Smad2 cells compared with sh-Control cells, demonstrating the requirement of Smad2 activation and role of TGF-β signaling in CNT fibrogenesis.

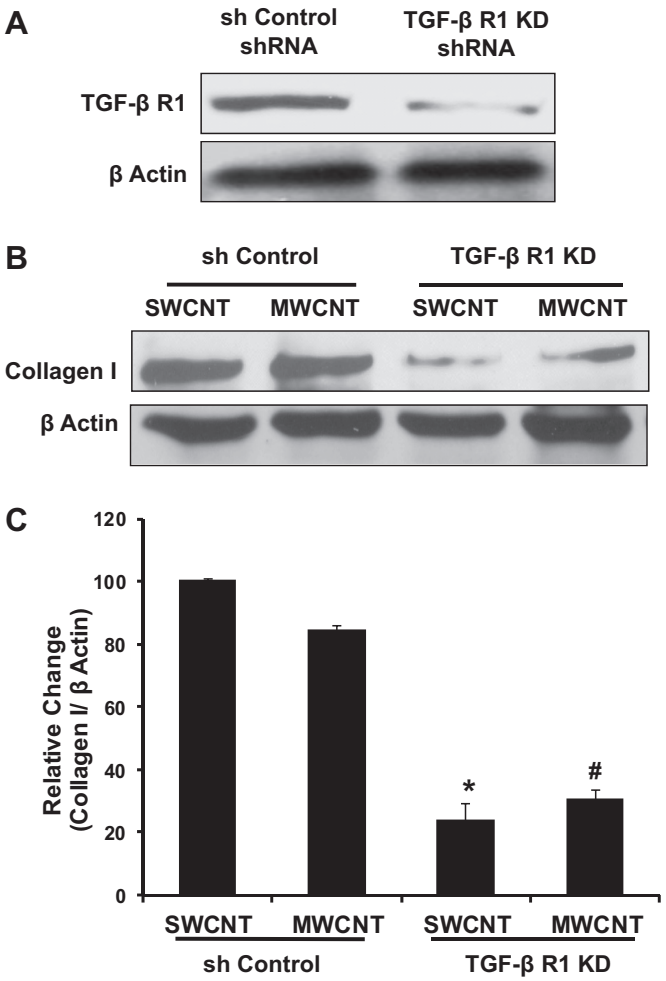

Fig. 6. Role of TGF-β R1 receptor in SWCNT and MWCNT-induced collagen expression. *A*: fibroblast CRL-1490 cells were transfected with TGF-β R1 short-hairpin (sh) RNA (sh-TGF-β R1) or control shRNA (sh-Control), and TGF-β R1 expression was analyzed by Western blotting. Representative blots are from $n = 3$ independent experiments. KD, knockdown. *B* and *C*: sh-Control and sh-TGF-β R1 cells were treated with 0.2 μg/cm^2 of SWCNT or MWCNT for 48 h. Collagen I expression was analyzed by Western blotting and quantified by densitometry (*C*). Representative blots from $n = 3$ independent experiments. Each bar represents the mean ± SD for $n = 3$ independent experiments. *$P < 0.05$ vs. SWCNT-treated sh-Control fibroblasts, #$P < 0.05$ vs. MWCNT-treated sh-Control fibroblasts.

DISCUSSION

Even though CNTs are widely studied for their pulmonary toxicity and fibrogenic effects, the underlying molecular mechanisms of their fibrogenic bioactivity are not fully understood (17, 18). Both SWCNT and MWCNT are known to penetrate and persist in pulmonary interstitial tissue, bringing them in direct contact with lung fibroblasts (22–24). This coincides with elevated TGF-β levels (27, 33). The present study shows that both lung epithelial and fibroblast cells produce TGF-β in response to CNT stimulation that activated a TGF-β/Smad2 pathway in lung fibroblasts, suggesting autocrine signaling in the cells. Importantly, our novel finding indicates the critical role of a TGF-β R1/Smad signaling pathway in the fibrogenic effect of CNTs in human lung cells. Identification of TGF-β R1 as a key player in CNT-induced activation of a fibrogenic signaling pathway will contribute to CNT lung fibrosis literature and suggests a potential cell surface marker for CNT-induced lung fibrosis.

In this study, aspiration of both SWCNT and MWCNT caused >3-fold increase in lung collagen I expression at 4 wk posttreatment compared with unexposed or UFCB-exposed

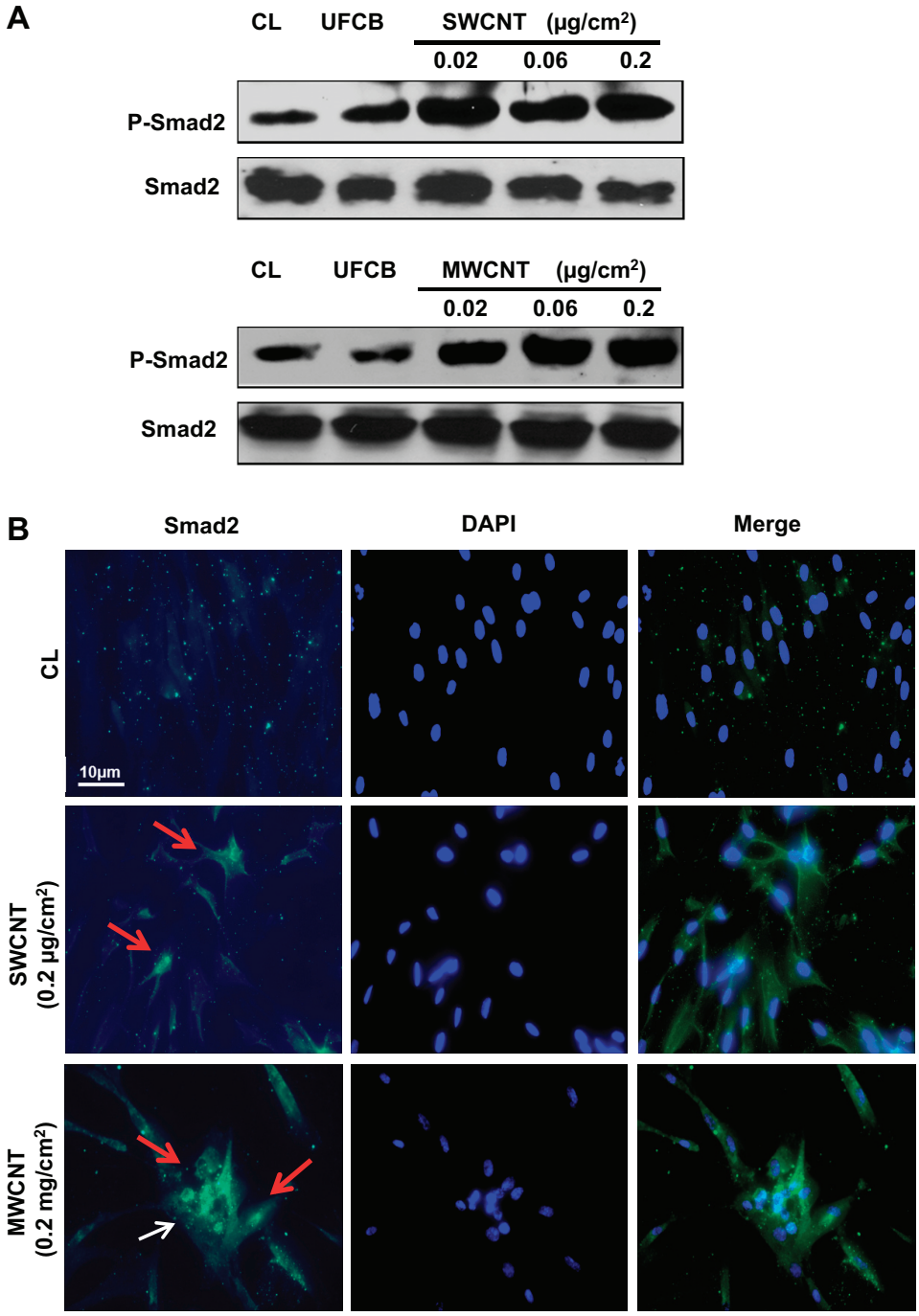

Fig. 7. Effects of SWCNT and MWCNT exposure on p-Smad2 expression and localization in lung fibroblasts. *A*: CRL-1490 cells were treated with 0.02–0.2 μg/cm^2 of SWCNT or MWCNT for 48 h and cell lysates were analyzed for Smad2 phosphorylation (p-Smad2; 42 kDa) and Smad2 (60 kDa) by Western blotting and compared with dispersant-only control (CL) and UFCB-treated cells. Representative blots are from $n = 3$ independent experiments. *B*: cells were exposed to SWCNT (*middle*) or MWCNT (*bottom*) for 48 h and stained with primary antibody for p-Smad2, followed by FITC-tagged secondary antibody. Immunofluorescence micrographs show p-Smad2 protein location (red arrow) and CNT agglomerates (white arrow) compared with basal p-Smad2 location (*top*, Control, CL). Representative images are from $n = 3$ independent experiments with at least 100 cells per condition in each experiment. Scale bar, 10 μm.

control mice. These results are in good agreement with several published in vivo studies showing an increase in pulmonary wall thickness due to increased collagen deposition (22, 24, 30, 37). In vivo CNT fate studies report that 90% aspirated 10 μg SWCNT (~0.02 μg/cm^2), 8% aspirated 80 μg MWCNT (0.02 μg/cm^2), and 21% inhaled 28.1 μg MWCNT (0.04 μg/cm^2) migrate into the airway interstitium 1 day after exposure (22, 25). These data suggest that lung fibroblasts are one of the major targets of CNT pulmonary exposure. Our in vitro study results on the induction of collagen I in cultured lung fibroblasts by SWCNT and MWCNT are consistent with those observed in vivo, suggesting a cellular mechanism that penetration of pulmonary exposed CNTs into the interstitium may directly stimulate fibroblasts to cause unusually rapid interstitial fibrosis. This also supports the use of an in vitro fibroblast cell model for prediction and rapid screening of CNTs and other nanomaterials for fibrogenicity.

Our results suggest a potential TGF-β1 autocrine signaling response during stimulation of fibroblast cells by CNTs. TGF-β1 plays an important role in lung fibrosis development, and multiple lung cell types, including epithelial cells and macrophages, are involved in the secretion of TGF-β1 after CNT exposure (26). Increasing evidence suggests that paracrine signaling from damaged epithelial cells promotes fibro-

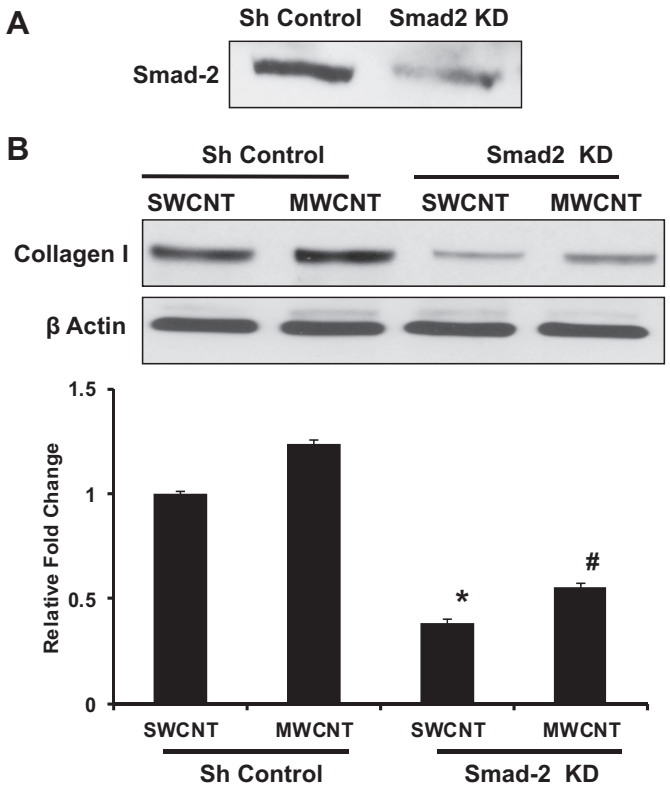

Fig. 8. Effect of SWCNT and MWCNT on collagen expression in Smad2 knockdown cells. *A*: CRL-1490 cells were transfected with Smad2 shRNA (sh-Smad2) or control shRNA (sh-Control) followed by analysis of Smad2 expression by Western blotting. *B*: sh-Control and Smad2 knockdown (KD) cells were treated with 0.2 μg/cm^2 of SWCNT or MWCNT for 48 h. Collagen I expression in both cells was measured by Western blotting. Representative blots are from $n = 3$ independent experiments. Each bar represents the mean ± SD for $n = 3$ independent experiments. *$P < 0.05$ vs. SWCNT-treated sh-Control cells, #$P < 0.05$ vs. MWCNT-treated sh-Control cells.

blast cell activation, which in turn further damages epithelial cells. This paracrine auto-feedback loop between different cell types is thought to contribute to progressive lung fibrosis. Macrophages and epithelial cells are key cellular sources of TGF-β production, typically resulting in the suppression of inflammatory cell activation and proliferation (29, 36). Given the ability of both SWCNT and MWCNT to rapidly penetrate and persist in lung interstitium, prolonged stimulation and release of latent TGF-β1 from fibroblasts, in close proximity to epithelial integrins and other nonproteolytic activators of latent TGF-β1, could potentially act as an autocrine and a bidirectional amplification signal for rapid collagen production by fibroblasts (43). The results from this study indicate that *1*) both lung epithelial cells (26) and fibroblasts produce a significant amount of TGF-β, suggesting a potential autocrine feedback loop for CNT induction of collagen production, and *2*) the in vitro lung cell models predict the in vivo TGF-β and collagen I response after CNT exposure.

We demonstrated for the first time in this study that CNTs induce a dose-dependent increase in TGF-β R1 expression in lung fibroblasts. Changes in TGF-β R1 expression or mutations contribute to the pathologic development of atherosclerosis and various forms of cancer (5). TGF-β receptor knockout animals exhibited decreased liver fibrosis (31). Given its key role in phosphorylation of Smad proteins, TGF-β R1 is the key regulator of signal-induced angiogenesis (4), which may also hold true for CNT-induced pulmonary fibrosis. Chemical inhibition of TGF-β R1 in vivo can suppress pulmonary fibrosis induced by bleomycin and TGF-β (6, 14), supporting our finding on the role of TGF-β R1 in CNT-induced fibrogenesis.

Interestingly, SWCNT-exposed fibroblasts showed enhanced TGF-β, TGF-β R1, and collagen production compared with MWCNT-exposed cells. The same SWCNT was previously found to have a more potent fibrogenic effect than MWCNT in mice, partly due to their increased tissue penetration and reduced macrophage clearance (24, 30). In addition, the high specific surface area of SWCNT (15–38 folds greater than that of MWCNT) potentially contributed to their enhanced collagen-inducing effect in vitro. Murray et al. (27) concluded that nanoparticle surface area significantly contributed to the enhanced inflammatory and fibrogenic effects of SWCNT compared with asbestos fibers. It is worth noting that surface area has increasingly become a more relevant dose metric for nanotoxicity studies (12). Alternatively, differences in settling rate between UFCB, SWCNT, and MWCNT in the in vitro exposure model potentially contributed to differences in internal dose (20, 40, 42).

Smad2 signaling is known to promote mesothelium cell transition to myofibroblasts following TGF-β exposure, possibly contributing to idiopathic pulmonary fibrosis (28). Activation of a TGF-β/Smad pathway was reported in epithelial-derived cells, suggesting the potential role for this pathway in SWCNT-induced EMT (9) and fibroblast-myofibroblast transformation (21). These studies, however, did not directly test the functional role and contribution of activated Smad2 to collagen production. In the present study, we demonstrated for the first time the functional role of TGF-β R1/Smad2 signaling pathway in CNT-induced collagen production in lung fibroblasts.

Conclusions. The results of this study support the potential novel mechanism of CNT-induced fibrogenesis through an upregulation of TGF-β receptors and direct autocrine activation of a TGF-β1/TGF-β R1/Smad signaling pathway. This finding fills the critical knowledge gap in CNT-induced fibrogenesis and may aid in the design of mechanism-based risk assessment and prevention strategies for CNT-induced lung fibrosis. The experimental models described in this study could potentially be used to develop methods for in vitro prediction of toxicity and rapid screening of CNT-like fibrogenic nanomaterials.

GRANTS

This work was supported by the National Institute for Occupational Safety and Health and grants of the National Occupational Research Agenda (NORA; FY08-12 LMW6) and Nanotechnology Research Center (NTRC; FY12-15), National Institutes of Health (National Heart, Lung, and Blood Institute HL-095579), and National Science Foundation (EPS-1003907).

DISCLAIMER

The findings and conclusions in this report are those of the authors and do not necessarily represent the views of the National Institute for Occupational Safety and Health.

DISCLOSURES

No conflicts of interest, financial or otherwise, are declared by the author(s).

AUTHOR CONTRIBUTIONS

A.M., Y.R., and L.W. conception and design of research; A.M. and R.R.M. performed experiments; A.M., R.R.M., and L.W. analyzed data; A.M., Y.R., and L.W. interpreted results of experiments; A.M. prepared figures; A.M., Y.R., and L.W. drafted manuscript; A.M., T.A.S., Y.R., V.C., and L.W. edited and revised manuscript; A.M., T.A.S., R.D., Y.R., V.C., and L.W. approved final version of manuscript.

REFERENCES

1. **Agostini C, Gurrieri C.** Chemokine/cytokine cocktail in idiopathic pulmonary fibrosis. *Proc Am Thorac Soc* 3: 357–363, 2006.
2. **Attisano L, Wrana JL.** Mads and Smads in TGFβ signalling. *Curr Opin Cell Biol* 10: 188–194, 1998.
3. **Attisano L, Wrana JL.** Signal transduction by the TGF-beta superfamily. *Science* 296: 1646–1647, 2002.
4. **Bertolino P, Deckers M, Lebrin F, ten Dijke P.** Transforming growth factor-beta signal transduction in angiogenesis and vascular disorders. *Chest* 128: 585S–590S, 2005.
5. **Blobe GC, Schiemann WP, Lodish HF.** Role of transforming growth factor beta in human disease. *N Engl J Med* 342: 1350–1358, 2000.
6. **Bonniaud P, Margetts PJ, Kolb M, Schroeder JA, Kapoun AM, Damm D, Murphy A, Chakravarty S, Dugar S, Higgins L, Protter AA, Gauldie J.** Progressive transforming growth factor beta1-induced lung fibrosis is blocked by an orally active ALK5 kinase inhibitor. *Am J Respir Crit Care Med* 171: 889–898, 2005.
7. **Bussy C, Pinault M, Cambedouzou J, Landry M, Jegou P, Mayne-L'hermite M, Launois P, Boczkowski J, Lanone S.** Critical role of surface chemical modifications induced by length shortening on multi-walled carbon nanotubes-induced toxicity. *Part Fibre Toxicol* 9: 46, 2012.
8. **Castranova V, Schulte PA, Zumwalde RD.** Occupational nanosafety considerations for carbon nanotubes and carbon nanofibers. *Acc Chem Res* 46: 642–649, 2012.
9. **Chang CC, Tsai ML, Huang HC, Chen CY, Dai SX.** Epithelial-mesenchymal transition contributes to SWCNT-induced pulmonary fibrosis. *Nanotoxicology* 6: 600–610, 2012.
10. **De Volder MF, Tawfick SH, Baughman RH, Hart AJ.** Carbon nanotubes: present and future commercial applications. *Science* 339: 535–539, 2013.
11. **Dennler S, Goumans MJ, ten Dijke P.** Transforming growth factor β signal transduction. *J Leukoc Biol* 71: 731–740, 2002.
12. **Donaldson K, Schinwald A, Murphy F, Cho WS, Duffin R, Tran L, Poland C.** The biologically effective dose in inhalation nanotoxicology. *Acc Chem Res* 46: 723–732, 2013.
13. **Gharaee-Kermani M, Phan SH.** Molecular mechanisms of and possible treatment strategies for idiopathic pulmonary fibrosis. *Curr Pharm Des* 11: 3943–3971, 2005.
14. **Giri SN, Hyde DM, Hollinger MA.** Effect of antibody to transforming growth factor beta on bleomycin induced accumulation of lung collagen in mice. *Thorax* 48: 959–966, 1993.
15. **Heldin CH, Miyazono K, ten Dijke P.** TGF-[beta] signalling from cell membrane to nucleus through SMAD proteins. *Nature* 390: 465–471, 1997.
16. **Inman GJ, Nicolás FJ, Callahan JF, Harling JD, Gaster LM, Reith AD, Laping NJ, Hill CS.** SB-431542 is a potent and specific inhibitor of transforming growth factor-β superfamily type I activin receptor-like kinase (ALK) receptors ALK4, ALK5, and ALK7. *Mol Pharmacol* 62: 65–74, 2002.
17. **Johnston HJ, Hutchison GR, Christensen FM, Peters S, Hankin S, Aschberger K, Stone V.** A critical review of the biological mechanisms underlying the in vivo and in vitro toxicity of carbon nanotubes: the contribution of physico-chemical characteristics. *Nanotoxicology* 4: 207–246, 2010.
18. **Kaiser JP, Roesslein M, Buerki-Thurnherr T, Wick P.** Carbon nanotubes - curse or blessing. *Curr Med Chem* 18: 2115–2128, 2011.
19. **Lanone S, Andujar P, Kermanizadeh A, Boczkowski J.** Determinants of carbon nanotube toxicity. *Adv Drug Deliv Rev* 65: 2063–2069, 2013.
20. **Li R, Wang X, Ji Z, Sun B, Zhang H, Chang CH, Lin S, Meng H, Liao YP, Wang M, Li Z, Hwang A, Song TB, Xu R, Yang Y, Zink JI, Nel AE, Xia T.** The surface charge and cellular processing of covalently functionalized multiwall carbon nanotubes determine pulmonary toxicity. *ACS Nano* 7: 2352–2368, 2013.
21. **Lin Z, Liu L, Xi Z, Huang J, Lin B.** Single-walled carbon nanotubes promote rat vascular adventitial fibroblasts to transform into myofibroblasts by SM22-alpha expression. *Int J Nanomedicine* 7: 4199–4206, 2012.
22. **Mercer R, Hubbs A, Scabilloni J, Wang L, Battelli L, Friend S, Castranova V, Porter D.** Pulmonary fibrotic response to aspiration of multi-walled carbon nanotubes. *Part Fibre Toxicol* 8: 21, 2011.
23. **Mercer R, Hubbs A, Scabilloni J, Wang L, Battelli L, Schwegler-Berry D, Castranova V, Porter D.** Distribution and persistence of pleural penetrations by multi-walled carbon nanotubes. *Part Fibre Toxicol* 7: 28, 2010.
24. **Mercer RR, Scabilloni J, Wang L, Kisin E, Murray AR, Schwegler-Berry D, Shvedova AA, Castranova V.** Alteration of deposition pattern and pulmonary response as a result of improved dispersion of aspirated single-walled carbon nanotubes in a mouse model. *Am J Physiol Lung Cell Mol Physiol* 294: L87–L97, 2008.
25. **Mercer RR, Scabilloni JF, Hubbs AF, Battelli LA, McKinney W, Friend S, Wolfarth MG, Andrew M, Castranova V, Porter DW.** Distribution and fibrotic response following inhalation exposure to multi-walled carbon nanotubes. *Part Fibre Toxicol* 10: 33, 2013.
26. **Mishra A, Rojanasakul Y, Chen BT, Castranova V, Mercer RR, Wang L.** Assessment of pulmonary fibrogenic potential of multiwalled carbon nanotubes in human lung cells. *J Nanomaterials* 2012: 11, 2012.
27. **Murray A, Kisin E, Tkach A, Yanamala N, Mercer R, Young SH, Fadeel B, Kagan V, Shvedova A.** Factoring-in agglomeration of carbon nanotubes and nanofibers for better prediction of their toxicity versus asbestos. *Part Fibre Toxicol* 9: 10, 2012.
28. **Nasreen N, Mohammed KA, Mubarak KK, Baz MA, Akindipe OA, Fernandez-Bussy S, Antony VB.** Pleural mesothelial cell transformation into myofibroblasts and haptotactic migration in response to TGF-beta1 in vitro. *Am J Physiol Lung Cell Mol Physiol* 297: L115–L124, 2009.
29. **Pelton RW, Johnson MD, Perkett EA, Gold LI, Moses HL.** Expression of transforming growth factor-beta 1, -beta 2, and -beta 3 mRNA and protein in the murine lung. *Am J Respir Cell Mol Biol* 5: 522–530, 1991.
30. **Porter DW, Hubbs AF, Mercer RR, Wu N, Wolfarth MG, Sriram K, Leonard S, Battelli L, Schwegler-Berry D, Friend S, Andrew M, Chen BT, Tsuruoka S, Endo M, Castranova V.** Mouse pulmonary dose- and time course-responses induced by exposure to multi-walled carbon nanotubes. *Toxicology* 269: 136–147, 2010.
31. **Qi Z, Atsuchi N, Ooshima A, Takeshita A, Ueno H.** Blockade of type beta transforming growth factor signaling prevents liver fibrosis and dysfunction in the rat. *Proc Natl Acad Sci USA* 96: 2345–2349, 1999.
32. **Ronzani C, Spiegelhalter C, Vonesch JL, Lebeau L, Pons F.** Lung deposition and toxicological responses evoked by multi-walled carbon nanotubes dispersed in a synthetic lung surfactant in the mouse. *Arch Toxicol* 86: 137–149, 2012.
33. **Ryman-Rasmussen JP, Tewksbury EW, Moss OR, Cesta MF, Wong BA, Bonner JC.** Inhaled multiwalled carbon nanotubes potentiate airway fibrosis in murine allergic asthma. *Am J Respir Cell Mol Biol* 40: 349–358, 2009.
34. **Sargent LM, Shvedova AA, Hubbs AF, Salisbury JL, Benkovic SA, Kashon ML, Lowry DT, Murray AR, Kisin ER, Friend S, McKinstry KT, Battelli L, Reynolds SH.** Induction of aneuploidy by single-walled carbon nanotubes. *Environ Mol Mutagen* 50: 708–717, 2009.
35. **Schinwald A, Murphy FA, Prina-Mello A, Poland CA, Byrne F, Movia D, Glass JR, Dickerson JC, Schultz DA, Jeffree CE, MacNee W, Donaldson K.** The threshold length for fiber-induced acute pleural inflammation: shedding light on the early events in asbestos-induced mesothelioma. *Toxicol Sci* 128: 461–470, 2012.
36. **Shull MM, Ormsby I, Kier AB, Pawlowski S, Diebold RJ, Yin M, Allen R, Sidman C, Proetzel G, Calvin D, Annunziata N, Doetschman T.** Targeted disruption of the mouse transforming growth factor-beta 1 gene results in multifocal inflammatory disease. *Nature* 359: 693–699, 1992.
37. **Shvedova AA, Kisin ER, Mercer R, Murray AR, Johnson VJ, Potapovich AI, Tyurina YY, Gorelik O, Arepalli S, Schwegler-Berry D, Hubbs AF, Antonini J, Evans DE, Ku BK, Ramsey D, Maynard A, Kagan VE, Castranova V, Baron P.** Unusual inflammatory and fibrogenic pulmonary responses to single-walled carbon nanotubes in mice. *Am J Physiol Lung Cell Mol Physiol* 289: L698–L708, 2005.
38. **Wang L, Castranova V, Mishra A, Chen B, Mercer R, Schwegler-Berry D, Rojanasakul Y.** Dispersion of single-walled carbon nanotubes by a natural lung surfactant for pulmonary in vitro and in vivo toxicity studies. *Part Fibre Toxicol* 7: 31, 2010.
39. **Wang L, Mercer RR, Rojanasakul Y, Qiu A, Lu Y, Scabilloni JF, Wu N, Castranova V.** Direct fibrogenic effects of dispersed single-walled carbon nanotubes on human lung fibroblasts. *J Toxicol Environ Health* 73: 410–422, 2010.

40. **Wang X, Xia T, Ntim SA, Ji Z, George S, Meng H, Zhang H, Castranova V, Mitra S, Nel AE.** Quantitative techniques for assessing and controlling the dispersion and biological effects of multiwalled carbon nanotubes in mammalian tissue culture cells. *ACS Nano* 4: 7241–7252, 2010.
41. **Wilson MS, Wynn TA.** Pulmonary fibrosis: pathogenesis, etiology and regulation. *Mucosal Immunol* 2: 103–121, 2009.
42. **Worsley KA, Kalinina I, Bekyarova E, Haddon RC.** Functionalization and dissolution of nitric acid treated single-walled carbon nanotubes. *J Am Chem Soc* 131: 18153–18158, 2009.
43. **Zhou Y, Hagood JS, Lu B, Merryman WD, Murphy-Ullrich JE.** Thy-1-integrin αvβ5 interactions inhibit lung fibroblast contraction-induced latent transforming growth factor-β1 activation and myofibroblast differentiation. *J Biol Chem* 285: 22382–22393, 2010.